Negative Sequence Compensation Method for High-Speed Railway With Integrated Photovoltaic Generation System

Xianfeng DAI, Minwu CHEN, Junhong LAI, Yingtao CHEN, Tianshu CHEN, and Ning ZHAO

Abstract—**The serious negative sequence (NS) issues and energy shortage problems are aroused by the single-phase 25-kV traction power supply system (TPSS) of high-speed railways. To achieve NS compensation and alleviation of energy demand, a TPSS with an integrated PV generation system is proposed. According to the structural characteristics of the TPSS and the PV system, a special topology and an NS compensation method are presented. Moreover, taking the NS control as the primary goal, three operation modes are classified by considering the load conditions of the TPSS and the output state of the PV system. After that, a coordinated control system with a central controller and multiple local controllers is proposed. The central controller can realize the flexible selection of operation modes and calculate the reference power. Meanwhile, the local controllers achieve the accurate tracking of the reference current and the stability of the DC link voltage by switching the control modes. Finally, the feasibility and effectiveness of the proposed system and the NS compensation method are verified by simulations.**

Index Terms—**Coordinated control, high-speed railway, negative sequence compensation, photovoltaic (PV), power quality.**

I. Introduction

ELECTRIFIED railway plays a key role in economic and social development as important national infrastructure. In recent years, the high-speed railway has achieved rapid development in China, connecting almost all provincial capitals and cities. However, on the one hand, the high-power load in the high-speed railway makes the negative sequence (NS) issue lead by single-phase 25-kV AC traction power supply systems (TPSSs) more serious, which arouses severe challenges for the reliability of the utility grid [1]−[3]. On the other hand, the development of the high-speed railway network makes the energy demand increase dramatically and will exacerbate the contradiction between supply and demand of energy [4].

To cope with the power quality problems dominated by NS, several compensation devices, such as static var compensator (SVC) [5], railway power conditioner (RPC) [6], modular multilevel converter (MMC) based RPC [7], power flow controller (PFC) [8], have been proposed. As one of the most popular utilization forms of clean energy, photovoltaic (PV) power generation has received extensive attention in recent years [9]. The AC TPSS represented by electrified railways has a natural intersection between the energy network and the transportation network. For example, the Qinghai-Tibet Railway passes through areas rich in solar energy resources in Northwest China, and there is a lot of idle land for development and utilization along the railway. Therefore, the PV power generation system is well suitable for connecting to the TPSS to ease the tension between the supply and demand of energy. Besides, the TPSS can not only effectively complete the nearby consumption of PV power, but also help expand the commercialization market of PV, which helps to economic benefits.

Consequently, research on connecting PV power generation systems to TPSSs has gradually become a hot spot. A solution to connect PV power generation system to the high-voltage 110 kV or 220 kV bus of a railway feeder station through a three-phase inverter was proposed, which does not need to modify the structure of the TPSS [10]. J. Aguado *et al.* [11] presented a direct access scheme on the traction side, where the PV system is directly connected to a certain phase traction feeder through a single-phase inverter. Although the structure is simple and robust, due to the asymmetric power supply structure on the traction side, it is easy to worsen the NS problem of the system during actual operation. P. Chen *et al.* [12] developed a V/V transformer-based scheme and an individual phase current control strategy with the hybrid current reference to integrate PV systems into TPSSs, where the locomotive was supplied by the asymmetrical part to mitigate the NS current, the surplus power was transferred back to the utility grid by the symmetrical part. However, when the generated power of the PV system is zero at night or in the early morning, the system cannot realize NS compensation. M. Wu *et al.* [13] designed a PV generation system for electrified railways based on a single-phase back-to-back converter, which absorbs PV energy while

Manuscript received June 30, 2021; revised September 8, 2021 and November 4, 2021; accepted December 23, 2021. Date of publication June 30, 2022; date of current version June 7, 2022. This work was supported by the National Natural Science Foundation of China under Grant 51877182. *(Corresponding author: Minwu Chen.)*

X. Dai, M. Chen, J. Lai, Y. Chen, and T. Chen are with the School of Electrical Engineering, Southwest Jiaotong University, Chengdu 611756, China (e-mail: daixf@my.swjtu.edu.cn; chenminwu@home.swjtu.edu.cn; 1121351893@qq.com; chenyt@my.swjtu.edu.cn; 565384263@qq.com).

N. Zhao is with the Birmingham Centre for Railway Research and Education, School of Electronic, Electrical and Computer Engineering, University of Birmingham, Birmingham, B15 2TT UK (e-mail: n.zhao@bham.ac.uk).

Digital Object Identifier 10.24295/CPSSTPEA.2022.00012

TABLE I
COMPARISON OF THE PROPOSED SCHEME AND SCHEMES IN THE LITERATURE

Literature	System scheme	NS compensation	Operation analysis	Dynamic performance
[4]	Mul ti-port RPC + PV (Complex)	√	√	About 2 grid cycles
[10]	Three-phase inverter and transformer + PV (Simple)	×	×	—
[11]	Single-phase inverter and transformer + PV (Simple)	×	×	—
[12]	Three-phase inverters + D/Y transformers + V/V transformer + PV (Complex)	√	×	—
[13]	RPC + 2 single-phase transformers + PV (Medium)	√	×	—
Study in this paper	3 single-phase inverters + Y/D transformer + PV (Simple)	√	√	About 1 grid cycle

suppressing NS. A multi-port RPC with a common low-voltage DC bus is proposed in [4], which can realize the efficient and concentrated access of large-scale PV generation compared to the conventional RPC in [13]. However, the multi-port RPC is structured with a cascaded multiple-active-bridge type, which needs a complex decoupling control strategy to attain well dynamic performance. Nevertheless, the above PV generation access schemes either only achieve NS compensation when the PV system is effectively outputting, or require additional compensation devices to enhance power quality. These methods neglect to control the reactive and active power flow of the system with PV inverters to compensate the NS current at any time and realize the consumption of PV energy.

Based on the analysis above, the TPSS integrated with a PV generation and an NS compensation method based on the PV inverters are presented in this paper. The main contributions of this paper can be summarized as follows:

1) Different from the conventional NS compensation configuration, the PV system is connected to the TPSS via three single-phase inverters, which have a simple topology and meet the limitation of power quality standards. And the corresponding compensation principle is given.
2) To achieve NS compensation during different scenarios, three operation modes of the system are divided, and their operat-ing characteristics and mutual conversion conditions are given, which can illustrate the transition process for different conditions.
3) A coordinated control strategy with a master-slave structure is given to obtain excellent dynamic behavior, which can imple-ment the seamless transition among different operation modes.

For a better understanding, a comparison of the study in the specified literature and the proposed scheme is given in Table I.

The rest of this paper is organized as follows: the system structure and the compensation principle are described in Section II. In Section III, the operation modes of the system are discussed in detail. Then the coordinated control strategy is proposed in Section IV. The simulation is carried out to verify the feasibility and effectiveness of the NS compensation method and control strategy in Section V. Finally, Section VI draws a conclusion.

II. Topology and Compensation Principle of the System

A. Topology of the System

The topology of the TPSS with integrated PV power genera-

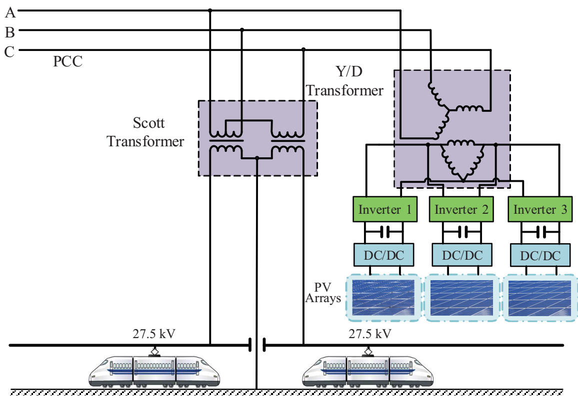

Fig. 1. Topology of the TPSS with an integrated PV power generation system.

tion system shown in Fig. 1 is composed of two parts. In the traction part, the Scott transformer is applied to transform the three-phase 110 kV voltage to single-phase 27.5 kV voltage, which can partly reduce the inherent NS issue of TPSSs due to the special structure. The PV power generation part consists of a step-up transformer, three single-phase grid-connected inverters and PV arrays. Concretely, the AC side of the single-phase grid-connected inverter is connected to the grid through the three-phase step-up transformer, and the DC side is directly connected to the DC/DC converter of PV arrays. Based on the above structure, the control unit performs coordinated control on each converter according to actual operating conditions. On the one hand, the inverters generate reasonable reactive power to deal with power quality problems; on the other hand, the inverters feed the active power back to the utility grid with its remaining capacity.

B. NS Compensation Principle

Due to the power factor of the high-speed electric multiple units (EMUs) nears to 1 now, only the NS compensation is analyzed here [14]. The NS limit at the point of common coupling (PCC) of the three-phase high-voltage side is taken as the compensation target. Compensation is achieved by controlling the reactive power injections of the inverters. And the active power of the inverters realizes three-phase symmetrical output, which does not participate in NS compensation. The total current of the traction load at the PCC is set as I_L, and the power of the traction load of the left arm greater than that of the

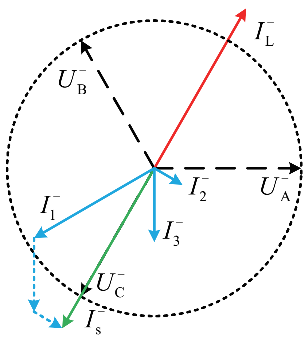

Fig. 2. Phasor diagram of NS compensation principle.

right arm is taken as an example for analysis.

Suppose the voltage of the power system is three-phase symmetrical, and take U_A as the reference phasor. For any traction port or compensation port λ on the secondary side of the transformer, the positive and negative sequence currents I_λ^+ and I_λ^- generated on the primary side can be expressed as: [15]

$$\begin{cases} I_\lambda^+ = \dfrac{1}{\sqrt{3}} k_\lambda I_\lambda e^{-j\varphi_\lambda} \\ I_\lambda^- = \dfrac{1}{\sqrt{3}} k_\lambda I_\lambda e^{-j(2\psi_\lambda+\varphi_\lambda)} \end{cases} \tag{1}$$

where I_λ is the effective value of the port current; ψ_λ is the angle at which the port voltage U_λ lags behind U_A, φ_λ is power factor angle, $k_\lambda = U_\lambda / \sqrt{3} U_A$.

The negative sequence phasor diagram of the compensation principle is shown in Fig. 2.

In Fig. 2, U_A^-, U_B^-, and U_C^- are NS phase voltage of the three phases A, B, and C, respectively. Furthermore, the reactive currents generated by grid-connected inverter 1, grid-connected inverter 2, and grid-connected inverter 3 are I_1, I_2, and I_3, and the corresponding NS currents are I_1^-, I_2^-, and I_3^-, respectively. Furthermore, the NS current I_L^- caused by the traction load can be offset with the NS current I_s^- synthesized by I_1^-, I_2^-, and I_3^-. When the NS is fully compensated, it can be formulated as:

$$I_L^- + I_s^- = I_L^- + I_1^- + I_2^- + I_3^- = 0 \tag{2}$$

By multiplying $3U_A$ by the conjugate complex number of the positive and negative sequence current in (1), the complex power of the positive and negative sequence of the three-phase system can be obtained

$$\begin{cases} S_\lambda^+ = S_\lambda e^{j\varphi_\lambda} \\ S_\lambda^- = S_\lambda e^{j(2\psi_\lambda+\varphi_\lambda)} \end{cases} \tag{3}$$

where $S_\lambda = U_\lambda I_\lambda$ is the apparent power of the port λ.

After being compensated by the grid-connected inverter, the NS power S^- at PCC can be expressed as:

$$S^- = S_L e^{j\theta_L} + \sum_{k=1}^{3} S_k e^{j\theta_k} \tag{4}$$

where $\theta_L = 2\psi_L + \varphi_L$, ψ_L is the angle at which the traction load voltage U_L lags behind U_A, φ_L is the power factor angle, which is regarded as 0 in this paper; $\theta_k = 2\psi_k + \varphi_k$, and ψ_k is the angle of the inverters' grid-connected voltage lagging behind U_A, φ_k is the power factor angle of the inverter k.

It can be inferred from Fig. 2. Phasor diagram of NS compensation principle.2 that the NS power caused by the load and the NS power caused by the inverters can cancel each other out. Therefore, the S^- can be also expressed as:

$$S^- = (1 - K_N) S_L e^{j\theta_L} \tag{5}$$

where K_N is defined as the NS compensation factor, and its value range is between 0 and 1, that is, $K_N \in [0,1]$.

According to (5), K_N can be expressed as:

$$K_N = \frac{-\sum_{k=1}^{3} S_k e^{j\theta_k}}{S_L e^{j\theta_L}} \tag{6}$$

where K_N is the ratio of the NS compensation power to the NS power at the PCC caused by the traction load.

ε is set as the expected value of the three-phase voltage unbalance degree at the PCC after compensation. According to the reference [16], the allowable value of NS power S_ε at the PCC is

$$S_\varepsilon = S_d \times \varepsilon \tag{7}$$

where S_d is the short-circuit capacity at PCC. When the S_ε is equal to the $|S^-|$, combining (5) and (7), K_N can be derived as:

$$K_N = 1 - \frac{S_d \times \varepsilon}{S_L} \tag{8}$$

It is worth noting that only the reactive power of the grid-connected inverters participates in the compensation. For the convenience of solving, it can be assumed that the grid-connected inverters only generate capacitive reactive power, that is, $\varphi_k = -\pi/2$. Therefore, the complex power of the inverters $S_k e^{j\varphi_k}$ can be expressed as:

$$S_k e^{j\varphi_k} = jS_k \sin\varphi_k = -jQ_k \tag{9}$$

where Q_k is the reactive power of the inverter k.

Then the NS power of the inverters can be formulated as:

$$S_k e^{j\theta_k} = -jQ_k e^{j2\psi_k} = Q_k e^{j(2\psi_k - \pi/2)} \tag{10}$$

Combining (6) and (10), expand the result according to the real and imaginary parts, the specific compensation model can be expressed as:

$$\begin{cases} K_N S_L \cos(2\psi_L) = -\sum_{k=1}^{3} Q_k \cos(2\psi_k - \pi/2) \\ K_N S_L \sin(2\psi_L) = -\sum_{k=1}^{3} Q_k \sin(2\psi_k - \pi/2) \end{cases} \tag{11}$$

There are three unknowns, Q_1, Q_2, Q_3, and only two equations, so an additional constraint is required to obtain a unique set. To avoid altering the reactive power demand of the system, the sum of the changes in reactive power injections is set equal to zero [17], which can be expressed as:

$$0=\sum_{k=1}^{3} Q_k \tag{12}$$

Combining (11) and (12), the final compensation model can be formulated as:

$$\begin{cases} K_{\mathrm{N}} S_{\mathrm{L}} \cos\left(2\psi_{\mathrm{L}}\right)=-\sum_{k=1}^{3} Q_k \cos\left(2\psi_k-\pi/2\right) \\ K_{\mathrm{N}} S_{\mathrm{L}} \sin\left(2\psi_{\mathrm{L}}\right)=-\sum_{k=1}^{3} Q_k \sin\left(2\psi_k-\pi/2\right) \\ 0=\sum_{k=1}^{3} Q_k \end{cases} \tag{13}$$

Based on the angle transformation formula, the (13) can be simplified as:

$$\begin{cases} K_{\mathrm{N}} S_{\mathrm{L}} \cos\left(2\psi_{\mathrm{L}}\right)=-\sum_{k=1}^{3} Q_k \sin\left(2\psi_k\right) \\ K_{\mathrm{N}} S_{\mathrm{L}} \sin\left(2\psi_{\mathrm{L}}\right)=\sum_{k=1}^{3} Q_k \cos\left(2\psi_k\right) \\ 0=\sum_{k=1}^{3} Q_k \end{cases} \tag{14}$$

where $\psi_{\mathrm{L}}=-\pi/6$, $\psi_1=2\pi/3$, $\psi_2=-2\pi/3$ and $\psi_3=0$ in the topology shown in Fig. 1. Correspondingly, Q_1, Q_2 and Q_3 can be solved by (15):

$$\begin{cases} Q_1=\dfrac{1}{\sqrt{3}} K_{\mathrm{N}} S_{\mathrm{L}} \\ Q_2=0 \\ Q_3=-\dfrac{1}{\sqrt{3}} K_{\mathrm{N}} S_{\mathrm{L}} \end{cases} \tag{15}$$

where $Q_k>0(k=1,2,3)$ means that the grid-connected inverter k outputs capacitive reactive power; otherwise, the grid-connected inverter k outputs inductive reactive power.

III. Discussion of Operation Mode

According to the output of PV power generation units, the PV power generation system is usually divided into the PV effective output condition and the PV no output condition. However, the operation modes of the TPSS connected with the PV power generation system not only depend on the output condition of the PV arrays but also relate to the traction load. In this paper, the apparent rated power S_{rate} of the grid-connected inverter is greater than the maximum power $P_{\mathrm{pv}}^{\max}$ of the PV units. An ideal assumption is made that the output power of the three PV arrays is the same at any time for simplifying the analysis. With NS compensation as the primary goal, the system can be classified into the following three operating modes according to the relationship between the generated power P_{pv} of the PV units, the traction load power S_{L}, and the rated power S_{rate} of the inverters. Moreover, the transition relationship among different modes is depicted in Fig. 3.

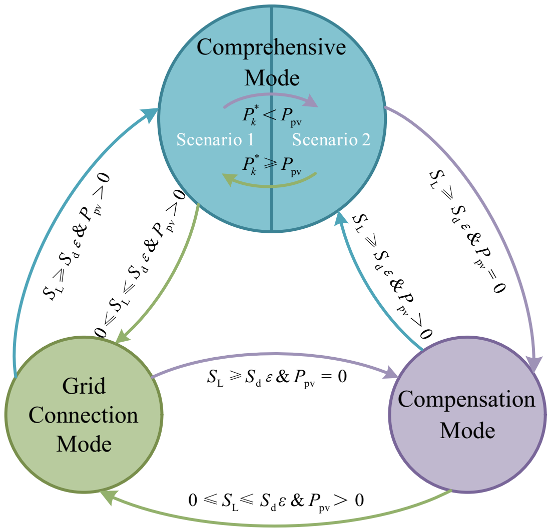

Fig. 3. Transition relationship among different operation modes.

A. Grid-Connection Operation Mode

In this mode, there is no traction load ($S_{\mathrm{L}}=0$) or NS caused by traction load at PCC that meets the requirements ($S_{\mathrm{L}}<S_{\mathrm{d}}\cdot\varepsilon$), and the PV power generation units work in the maximum power point tracking (MPPT) mode to achieve maximum power tracking. The grid-connected inverters do not generate reactive power for NS compensation, and only active power is delivered to the utility grid. Therefore, the active reference power P_k^{ref} of the grid-connected inverter k can be expressed as:

$$P_k^{\mathrm{ref}}=P_{\mathrm{pv}} \tag{16}$$

B. Comprehensive Operation Mode

The system gives priority to ensuring the demand for power quality control in this mode. First, the reactive reference power Q_k^{ref} of grid-connected inverter k for compensation can be obtained from (15). Then due to the capacity of inverters being fixed, its active power must satisfy the limit (17).

$$P_k=\sqrt{\left(S_{\mathrm{rate}}\right)^2-\left(Q_k^{\mathrm{ref}}\right)^2} \tag{17}$$

In order to prevent the active power of the inverters from causing additional NS at PCC, the active power P_k^* of the grid-connected inverter k should satisfy (18).

$$P_k^*=\min\left(P_k\right) \tag{18}$$

Moreover, this mode contains two scenarios: (i) when

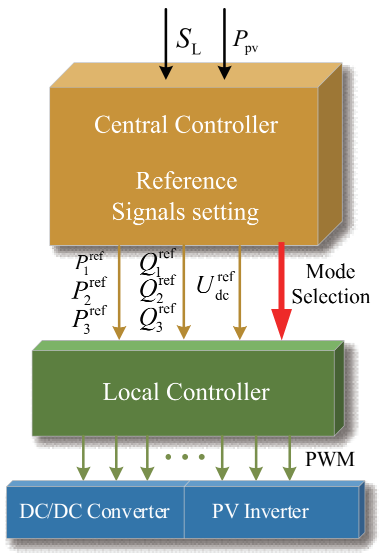

Fig. 4. Structure of proposed coordinated control strategy.

$P_k^* \geqslant P_{pv}$, the DC/DC converters perform MPPT control to realize maximum power tracking. The active reference power P_k^{ref} of the grid-connected inverter k is equal to P_{pv}. (ii) When $P_k^* \geqslant P_{pv}$, the DC/DC converters quits the MPPT control mode and switches to the constant voltage control (CVC) mode to stable the DC bus voltage. Furthermore, the active reference power P_k^{ref} of the PV inverter k can be expressed as:

$$P_k^{ref} = P_k^* \tag{19}$$

C. Compensation Operation Mode

This is a special mode that operates when the generated power of the PV system is zero ($P_{pv} = 0$) at night or in the early morning. The PV power units are on standby, and when the TPSS is loaded ($S_L < S_d \cdot \varepsilon$), the grid-connected inverters only generate reactive power by switching the control mode to compensate for the NS. In addition, when the DC bus voltage is too large or too small, the inverter exchanges a small amount of active power with the grid to stabilize the DC bus voltage to ensure the normal operation of the devices.

IV. Coordinated Control Strategy

In order to achieve the effective control of power quality and the efficient consumption of PV energy, as well as to realize the rapid conversion between three operation modes, a coordinated control strategy with a master-slave structure is proposed. The proposed coordinated control system is composed of a central controller and multiple local controllers, as depicted in Fig. 4.

A. Central Controller

First, the central controller calculates the reference value of the inverters' output active power and reactive power based on the detected real-time voltage and current data of the traction side and the PV side. Then it selects the operating mode and transmits the corresponding active power and reactive power reference values and the DC link voltage setting value to the local controllers. This process is based on the mode division introduced in Section III. Finally, the local controllers combine the reference signal sent by the central controller and the locally detected voltage and current signals to complete the precise control of the controlled objects.

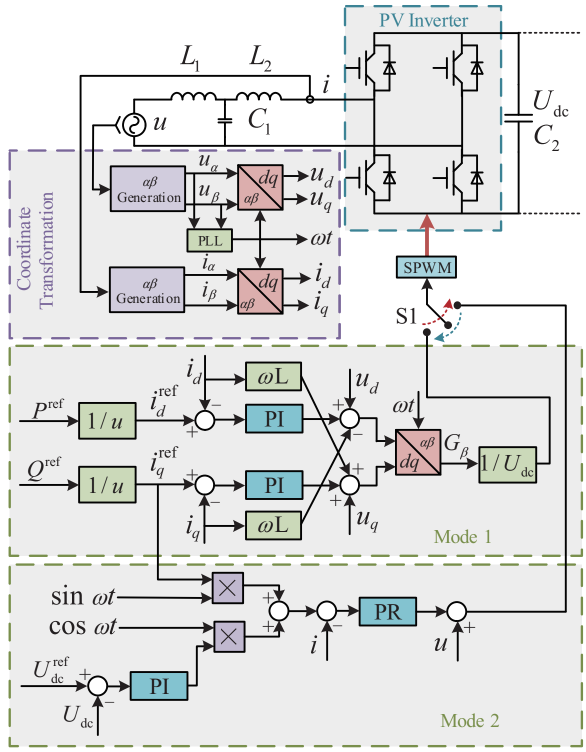

Fig. 5. The comprehensive control method of the inverter.

B. Local Controller

1) The Control Method of the PV Inverter

As shown in Fig. 5, an LCL filter is installed at the output of the inverter, which can effectively filter out the harmonic components in the grid-connected current. To implement the compensation of the NS at the PCC under different operating modes, a comprehensive control method with two control modes for PV inverters is proposed. When the system works in the first two operating modes, the central controller makes the inverter controller operate in control mode 1 through switch S1; when the system works in the third operating mode, the local controller switches to control mode 2. The control mode 1 realizes the *dq* current decoupling control of the single-phase inverters by constructing a two-phase quadrature signal for Park coordinate transformation, which achieves the separate and precise control of the active and reactive power of the grid-connected inverters. In the compensation operating mode, the output power of PV is zero, and the inverters need to exchange a small amount of active power with the grid to stabilize the DC link voltage. In control mode 2, the proportional-integral (PI) control of the DC link voltage ensures the normal operation of the inverter. Since the single-phase current signal is a sinusoidal signal of power frequency and multiplied

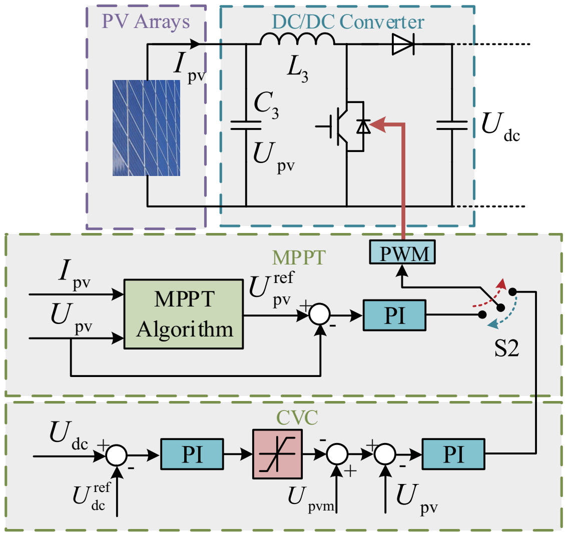

Fig. 6. The comprehensive control method of the DC/DC converter.

frequency, proportional resonance (PR) control is used to achieve no static error tracking of single-phase current.

2) The Control Method of the DC/DC Converter

The control structure of the PV system is shown in Fig. 6, where it consists of MPPT mode and CVC mode. Generally, the PV system runs in MPPT mode to improve solar energy utilization efficiency, but when the output power of the inverter is less than the PV power, in order to prevent the DC link voltage from rising continuously, the central controller controls it to operate in CVC mode through switch S2. The MPPT mode is controlled by the perturbation and observation method, in view of the relative maturity of existing researches, it will not be repeated herein. For the CVC mode, an improved dual-loop control strategy is adopted to fix the PV output voltage U_{pv} to the left of the maximum power point voltage U_{pvm} during CVC, which makes the system more stable compared to the traditional CVC [18].

V. Simulation

To verify the feasibility and correctness of the proposed topology and control strategy, a simulation model corresponding to the topology presented in Fig. 1 is constructed on Matlab/Simulink software. A set of different imbalance scenarios are designed to verify the effectiveness of the NS compensation strategy. Besides, a continuous operating case with three different operation modes is simulated to demonstrate the effectiveness of the coordinated control strategy. To highlight the effect of NS compensation, the extreme situation in which one power supply arm has a load and the other power supply arm has no load is simulated. The detailed parameters of the system and the control parameters are shown in Table II and Table III, respectively.

The inverters only perform NS compensation in the compensation operation mode, which is suitable to verify the effectiveness of the compensation strategy. The simulation

TABLE II
Main Circuit Parameters

Items	Parameters	Value
Utility grid	Voltage level	110 kV
	Short-circuit capacity	750 MVA
Transformer	Scott transformer capacity	10 MVA
	Scott transformer ratio	110/27.5
	Y/D transformer capacity	10 MVA
	Y/D transformer ratio	110/5
PV system	Grid-connected inverter capacity	3 MVA
	DC bus voltage reference value	8 kV
	Maximum power point voltage	1660 V
	Maximum output power of PV arrays	2.14 MWp
	L_1	2.35 mH
	L_2	2.06 mH
	L_3	7.5 mH
	C_1	6 μF
	C_2	5 mF
	C_3	3.5 mF

TABLE III
Parameters of Control

Items	Parameters	Value
Control mode 1	K_P	50
	K_I	3850
Control mode 2	K_{P1}	1.8
	K_I	200
	K_{P2}	10
	K_R	400
MPPT mode	K_P	0.0075
	K_I	0.075
CVC mode	K_{P1}	0.2
	K_{I1}	2
	K_{P2}	0.01
	K_{I2}	0.03

TABLE IV
Parameters in Different Unbalanced Scenarios

Parameters	Case 1	Case 2	Case 3	Case 4
Time/s	0–0.1	0.1–0.2	0.2–0.3	0.3–0.4
Load location	Left arm	Left arm	Right arm	Right arm
S_L /MW	3.00	5.00	5.00	4.00
K_N	0.5	1	0.8	1

during different unbalanced scenarios consists of four cases, which correspond to the two situations that the load on the left power arm is greater than the right one or the load on the right power arm is greater than the left one in practice. Moreover, the NS compensation factor K_N among these cases is set to different values, the details of the cases are shown in Table IV.

It can be observed from Fig. 7 that the proposed compensa-

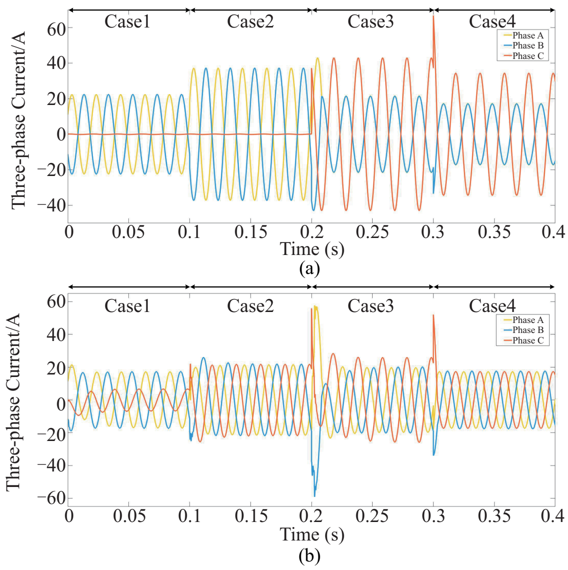

Fig. 7. The three-phase current at the PCC. (a) Before compensation. (b) After compensation.

TABLE V
SIMULATION POWER IN CONTINUOUS CASE

Parameters	Case 1	Case 2	Case 3	Case 4
Time/s	0−0.2	0.2−0.4	0.4−0.6	0.6−0.8
P_{pv}^{max} /MW	2.14	1.07	2.14	0
S_L /MW	0	4.00	4.00	5.00

tion strategy can effectively compensate the NS current of the system according to the expected value (K_N).

The continuous operating case consisting of four operating cases is designed to demonstrate the excellent performance of the system in terms of NS suppression and PV consumption, as well as to evaluate the system's dynamic performance changing from one operation mode to another. The NS compensation factor K_N is set to 1, that is, the NS is fully compensated. The details of the designed case are shown in Table V.

During $t \in (0\text{ s}, 0.2\text{ s})$, the TPSS is unloaded and the PV system performs MPPT to generate its maximum output power of 2.14 MW, which corresponds to the grid-connection operation mode of the system. In case 2 ($t \in (0.2\text{ s}, 0.4\text{ s})$), the traction power is 4 MW and the PV system is still tracking the maximum power point, but its maximum output power drops to 1.07 MW due to the decrease of the solar irradiance. The system is now in the first scenario of the comprehensive operation mode. During $t \in (0.4\text{ s}, 0.6\text{ s})$, the traction power is still 4 MW and the maximum output power of the PV system is restored to 2.14 MW. However, due to the capacity limitation of inverters, the maximum PV output power is greater than the reference active power output of a single inverter. The PV system performs CVC mode and its actual output power should track the active power generated by the inverter, which corresponds to the second scenario in the comprehensive operation mode. The traction power is increased to 5 MW and the solar irradiance is reduced to 0 W/m^2 after $t = 0.6$ s. The PV

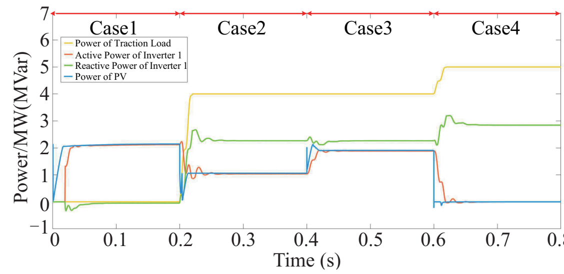

Fig. 8. Power allocation of the system.

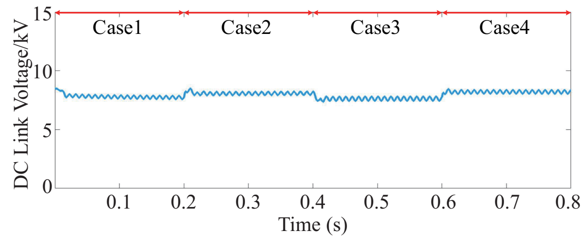

Fig. 9. DC link voltage of the PV system.

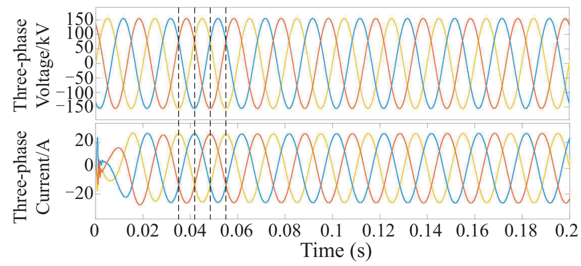

Fig. 10. The voltage and current at the PCC in grid-connection mode.

system is on standby, inverters only generate reactive power for compensation, and the system is in compensation operation mode.

The PV power generation system where the grid-connected inverter 1 is located is taken as an example to analyze the simulation results. As observed in Fig. 8, the power of the system can be accurately allocated as expected under different working cases. Especially, the PV system has just switched from MPPT control mode to CVC control mode at 0.4 s. Therefore, in the first short period of case 3, the PV system generates its maximum output power (2.14 MW), and then quickly tracks the inverter's output power (1.91 MW) with the control of CVC, as displayed in Fig. 8. and 9 shows that the dc-link voltage of the PV system is effectively maintained around its reference value and there is no severe transient behavior under the variation situation of the inverter power and PV output power.

Figs. 10 and 11 illustrate in detail the condition of the three-phase voltage and three-phase current at the PCC in grid-connection operation mode and compensation operation mode, respectively. The phase of the three-phase voltage and the three-phase current are opposite shown as Fig. 10, indicating that the PV system is feeding energy back to the utility grid

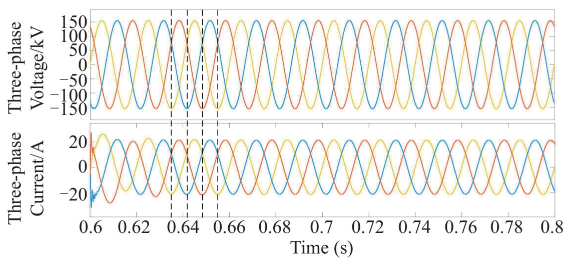

Fig. 11. The voltage and current at the PCC in compensation mode.

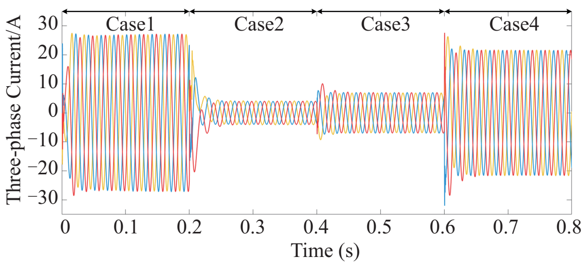

Fig. 12. The three-phase current at the PCC in the continuous operating case.

through the inverters. In Fig. 11, the phase of the three-phase voltage and the three-phase current are the same, indicating that the TPSS is getting power from the utility grid.

In addition, Fig. 12 depicts the condition of the three-phase current at the PCC of the high-voltage side. It is easy to observe that the three-phase primary currents of the high-voltage side are symmetrical no matter what the operation cases are, which achieves the established compensation target.

The above simulation results display that the three-phase currents at PCC are symmetric in all cases and the PV energy can be effectively utilized. Furthermore, the simulation results also suggest that the system possesses excellent dynamic behavior with the coordinated control strategy. Because it can return to a steady-state from one operating condition to another in a short period of time (about 1 main grid period).

VI. Conclusion

This paper presents a single-phase inverter-based TPSS with an integrated PV generation system and its NS compensation method, which achieves the compensation with the reactive power current generated by the inverters. According to the characteristics of TPSSs and PV systems, the proposed system is divided into three operating modes. In addition, a coordinated control system with a central controller and multiple local controllers is proposed. The central controller achieves flexible selection of the system operation modes and calculation of reference power. the local controllers coordinate to track the reference current and stabilize the DC link voltage according to the command of the central controller. Finally, the simulation results show that the topology and control strategy proposed based on the NS compensation method can effectively achieve NS compensation and alleviate energy demand with the absorption of PV energy.

References

[1] H. Hu, Z. He, X. Li, K. Wang, and S. Gao, “Power-quality impact assessment for high-speed railway associated with high-speed trains using train timetable—Part I: Methodology and modeling,” in *IEEE Transactions on Power Delivery*, vol. 31, no. 2, pp. 693–703, Apr. 2016.

[2] Y. Chen, M. Chen, Z. Tian, Y. Liu, and S. Hillmansen, “VU limit pre-assessment for high-speed railway considering a grid connection scheme,” in *Iet Generation Transmission Distribution*, vol. 13, no. 7, pp. 1121–1131, Apr. 2019.

[3] Y. Chen, M. Chen, Z. Tian, and Y. Liu, “Voltage unbalance management for high-speed railway considering the impact of large-scale DFIG-based wind farm,” in *IEEE Transactions on Power Delivery*, vol. 35, no. 4, pp. 1667–1677, Aug. 2020

[4] F. Ma, X. Wang, L. Deng, Z. Zhu, Q. Xu, and N. Xie, “Multiport railway power conditioner and its management control strategy with renewable energy access,” in *IEEE Journal of Emerging and Selected Topics in Power Electronics,* vol. 8, no. 2, pp. 1405–1418, Jun. 2020.

[5] G. Zhu, J. Chen, and X. Liu, “Compensation for the negative sequence currents of electric railway based on SVC,” in *Proceedings of the 3rd IEEE Conference on Industrial Electronics and Applications*, Singapore, 2008, pp. 1958–1963.

[6] F. Ma, A. Luo, X. Xu, H. Xiao, C. Wu, and W. Wang, “A simplified power conditioner based on half-bridge converter for high-speed railway system,” in *IEEE Transactions on Industrial Electronics*, vol. 60, no. 2, pp. 728–738, Feb. 2013.

[7] F. Ma, Q. Xu, Z. He, C. Tu, Z. Shuai, A. Luo, and Y. Li, “A railway traction power conditioner using modular multilevel converter and its control strategy for high-speed railway system,” in *IEEE Transactions on Transportation Electrification*, vol. 2, no. 1, pp. 96–109, Mar. 2016.

[8] M. Chen, Q. Li, C. Roberts, S. Hillmansen, P. Tricoli, N. Zhao, and I. Krastev, “Modelling and performance analysis of advanced combined co-phase traction power supply system in electrified railway,” in *Iet Generation Transmission & Distribution*, vol. 10, no. 4, pp. 906–916, Mar. 2016.

[9] F. Mancini and B. Nastasi, “Solar energy data analytics: PV deployment and land use,” in *Energies*, vol. 13, no. 2, p. 417, Jan. 2020.

[10] S. D’Arco, L. Piegari, and P. Tricoli, “Comparative analysis of topologies to integrate photovoltaic sources in the feeder stations of AC railways,” in *IEEE Transactions on Transportation Electrification*, vol. 4, no. 4, pp. 951–960, Dec. 2018.

[11] J. Aguado, A. J. Sánchez-Racero, and S. de la Torre, “Optimal operation of electric railways with renewable energy and electric storage systems,” in *IEEE Transactions on Smart Grid*, vol. 9, no. 2, pp. 993–1001, Mar. 2018.

[12] P. Chen, C. Wu, H. Kong, F. Blaabjerg, and Y. Quan, “Connection and control strategy of PV converter integrated into railway traction power supply system,” in *Energies*, vol. 13, no. 22, p. 5989, Nov. 2020.

[13] M. Wu, W. Wang, W. Deng, H. Chen, C. Dai, and W. Chen, “Back-to-back PV generation system for electrified railway and its control strategy,” in *IEEE Asia-Pacific Transportation Electrification Conference and Exposition*, Harbin, China, 2017, pp. 244–249.

[14] K. Wang, H. Hu, Z. Zheng, Z. He, and L. Chen, “Study on power factor behavior in high-speed railways considering train timetable,” in *IEEE Transactions on Transportation Electrification*, vol. 4, no. 1, pp. 220–231, Mar. 2017.

[15] S. Xie, Y. Zhang, and H. Wang, “A novel co-phase power supply system for electrified railwaybased on V type connection traction transformer,” in *Energies*, vol. 14, no. 4, p. 1214, Feb. 2021.

[16] M. Chen, Y. Cheng, Z. Cheng, D. Zhang, Y. Lv, and R. Liu, “Energy storage traction power supply system and control strategy for an electrified railway,” in *Iet Generation Transmission Distribution*, vol. 14, no. 12, pp. 2304–2314, Jun. 2020.

[17] S. -Y. Lee and C. -J. Wu, “On-line reactive power compensation schemes for unbalanced three phase four wire distribution feeders,” in *IEEE Transactions on Power Delivery*, vol. 8, no. 4, pp. 1958–1965, Oct. 1993.

[18] Q. Cheng, W. Sun, Y. Cheng, L. Chen, and T. Li, “Improved constant voltage control of PV power generation system in DC microgrid,” in *Acta Energiae Solaris Sinica*, vol. 44, no. 11, pp. 320-330, Nov. 2019.

Xianfeng Dai received the B.Eng. degree in electrical engineering and automation from Shenyang Jianzhu University, Shenyang, China, in 2020. He is currently pursuing the M.Sc. degree in electrical engineering with Southwest Jiaotong University, Chengdu, China.

His current research interests include railway power traction systems, integration of renewable energy source and energy storage system, and power quality control.

Minwu Chen received the B.Eng. and Ph.D. degrees in electrical engineering from Southwest Jiaotong University, Chengdu, China, in 2004 and 2009, respectively, all in electrical engineering.

From 2010 to 2012, he undertook postdoctoral researches in the China Railway First Survey and Design Institute Group, Xi'an, China. Since 2018, he has been a Full Professor at the School of Electrical Engineering, Southwest Jiaotong University, and is currently the Vice Dean of School of Electrical Engineering. From 2014 to 2015, he was a Visiting Scholar at the University of Birmingham, Birmingham, UK. His research interests include new technology and power quality for railway traction systems.

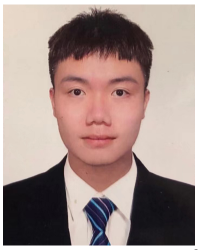

Junhong Lai received the B.Eng. in electrical engineering and automation from Southwest Jiaotong University, Chengdu, China, in 2020. He is now pursuing the M.Sc. degree in electrical engineering with the College of Electrical Engineering, Southwest Jiaotong University, Chengdu, China.

His current research interests include power quality improvement, integration of renewable energy source and energy storage system, and energy management strategy of the electric traction system.

Yingtao Chen received the B.Eng. in electrical engineering and automation from Southwest Jiaotong University, Chengdu, China, in 2019, where he is currently pursuing the M.S. degree in College of Electrical Engineering. His current research interests include railway traction systems and power quality control.

Tianshu Chen received the B.Eng. degree in electrical engineering from Southwest Jiaotong University, Chengdu, China, in 2021, where he is currently working toward the M.S. degree in electrical engineering. His research interests include railway traction systems and converter control.

Ning Zhao received M.Sc. and Ph.D. degrees in electronic, electrical and computer engineering from the University of Birmingham in 2009 and 2013 respectively.

He is a Postdoctoral Research Fellow at the University of Birmingham's Centre for Railway Research and Education. His main research area includes railway energy saving, railway system modelling, train trajectory optimization and optimization techniques.